Radial *S* wave velocity structure of the D" region under a spot of the east central Pacific Ocean

Luis F. Terán-Mendieta and Raúl W. Valenzuela[*]

Resumen

Se determinó la estructura radial de velocidades para la onda *S* en la base del manto en un área del Océano Pacífico centro-oriental centrada en los 19°N, 132°O. Se aplicó la técnica de la constante de disipación en el dominio de la frecuencia a las ondas *S* y S_{diff} de un sismo producido en las islas Tonga y registrado en el noreste de los Estados Unidos. Se trabajó con 29 modelos diferentes, entre los cuales se incluían modelos con una discontinuidad de la velocidad y también el Modelo Preliminar de Referencia de la Tierra (PREM). De acuerdo con el ajuste a la constante de disipación en el dominio de la frecuencia y a las formas de onda en el dominio del tiempo, se consideró que PREM es el mejor modelo. Esto implica que en esta ubicación D" tiene un espesor de 150 km y un gradiente de velocidad ligeramente negativo conforme aumenta la profundidad. No se encontró una discontinuidad de la velocidad en la parte superior de D". La estructura de velocidades observada es consistente con el comportamiento de D" como una capa térmica limítrofe y también con la posibilidad de que el material del manto se enriquezca en hierro como consecuencia de reacciones químicas con el núcleo. Además este modelo sugiere que en esta región existen temperaturas ligeramente elevadas en la base del manto. Por otra parte, no se esperaría encontrar una discontinuidad en esta zona puesto que ahí no se ha producido subducción en los últimos 180 millones de años.

Palabras clave: ondas difractadas, interfaz núcleo-manto, D", constante de disipación, post-perovskita, capa térmica limítrofe.

Abstract

The *S* wave radial velocity structure at the base of the mantle was constrained for an area of the east central Pacific Ocean centered at 19°N, 132°W. The decay constant technique was applied in the frequency domain to the *S* and S_{diff} waves of an earthquake in the Tonga Islands recorded in the northeastern United States. A total of 29 different *S* wave velocity models were explored, including models with a velocity discontinuity and also the Preliminary Reference Earth Model (PREM). As determined from the fit to the decay constant in the frequency domain and to the waveforms in the time domain, PREM was considered the best model. This choice implies that D" at this location is 150 km thick and has a slightly negative velocity gradient with increasing depth. No velocity discontinuity was found at the top of D". The proposed velocity structure is consistent with D" acting as a thermal boundary layer and also with the possible existence of mantle enriched in iron through chemical reactions with the core. The preferred model also implies the existence of slightly elevated temperatures at the base of the mantle. The lack of a discontinuity is consistent with the absence of subduction at this location during the last 180 Myr.

Key words: diffracted waves, core-mantle boundary, D", decay constant, post-perovskite, thermal boundary layer.

L.F. Terán-Mendieta
Departamento de Sismología
Instituto de Geofísica
Universidad Nacional Autónoma de México
Ciudad Universitaria
Delegación Coyoacán, 04510
México D.F., México

Now at Colegio de Ciencias y Humanidades Plantel Sur
Universidad Nacional Autónoma de México
México D.F., México
E-mail: luisteran@yahoo.com

R. W. Valenzuela[*]
Instituto de Geofísica
Universidad Nacional Autónoma de México
Ciudad Universitaria
Delegación Coyoacán, 04510
México D.F., México
[*]Corresponding author: raul@ollin.igeofcu.unam.mx

Introduction

A number of different approaches have been pursued in order to determine the velocity structure at the base of the mantle. Core diffracted waves are well suited for studying the velocity at the core-mantle boundary (CMB) because they spend a significant portion of their paths at this interface. Two techniques in particular involve the use of the ray parameter (Doornbos and Mondt, 1979b; Mula and Müller, 1980; Doornbos, 1983; Valenzuela-Wong, 1996; Valenzuela and Wysession, 1998; Valenzuela *et al.,* 2000) and the decay constant (Doornbos and Mondt, 1979a, 1979b; Mula, 1981; Doornbos, 1983; Valenzuela-Wong, 1996; Valenzuela and Wysession, 1998). By measuring the ray parameter in the time domain it is possible to determine the lateral velocity structure at the base of the mantle. On the other hand, the robust decay constant method relies on the frequency domain amplitude decay of diffracted waves and is sensitive to the radial velocity structure. Early work using the decay constant led some investigators to the conclusion that D" has a negative velocity gradient for both *P* and *S* waves (Mondt, 1977; Doornbos and Mondt, 1979b; Doornbos, 1983), while other researchers found slightly positive gradients (Mula and Müller, 1980; Mula, 1981). The velocity structure determined by these studies was based on the assumption that D" is globally homogeneous, which justified averaging the observations from individual earthquakes around the world. Wright and Lyons (1981) proposed a model with a discontinuous *P*-wave velocity increase for a region under the Caribbean Sea. Lay and Helmberger (1983) introduced several discontinuous shear wave velocity models for three different regions. It has been further suggested that the discontinuity is a global feature (Lay and Helmberger, 1983; Nataf and Houard, 1993; Sidorin *et al.,* 1999a; Sun and Helmberger, 2008). Although this discontinuity seems to be highly heterogeneous and it has not been observed everywhere, it has now been reported in many studies; see Nataf and Houard (1993), Krüger *et al.* (1995), Loper and Lay (1995), Wysession *et al.* (1998), Helmberger *et al.* (2005), Lay and Garnero (2007, 2011), Garnero and McNamara (2008), and Wookey and Dobson (2008) for a review. One of the leading explanations for the discontinuity is the occurrence of a phase transition from perovskite to post-perovskite under lowermost mantle conditions (Murakami *et al.,* 2004).

Given the uneven distribution of sources and receivers on a global scale, our sampling of the core-mantle boundary is not uniform. Of all the phases used to study D", core diffracted waves are the best suited for on-land recording, especially in eastern North America and southern Africa (Wysession, 1996a). The Missouri to Massachusetts (MOMA) array was in a very favorable location for recording diffracted waves from earthquakes in the southwest Pacific (Wysession *et al.,* 1996; Fischer *et al.,* 1996). This study presents the results of forward modeling the radial velocity structure at the base of the mantle in a spot under the east central Pacific Ocean using *SH* and SH_{diff} waves recorded by the MOMA array. Other authors (e. g., Sun and Helmberger, 2008; Kawai and Geller, 2010) have taken advantage of the new data gathered by the Transportable Array component of the USArray (Ammon and Lay, 2007) in order to obtain improved models of D" structure using various seismic phases.

Calculating the decay constant

This derivation follows from the work of Mula (1981); the theory is also described by van Loenen (1988) and Valenzuela-Wong (1996). Mathematically, the amplitude of the impulse recorded by a station at an epicentral distance Δ and azimuth ϕ from the source can be described in the frequency domain by the product of the following terms:

$$A(\omega, \varphi, \Delta) = S(\omega) \, R(\varphi, \Delta) \, M_{\text{d}}(\omega, \varphi) \, C(\omega, \varphi, \Delta) \\ M_{\text{u}}(\omega, \varphi) \, U(\omega) \, I(\omega), \tag{1}$$

where ω is angular frequency, $S(\omega)$ is the source time function, assuming that directivity effects are not significant, and $R(\phi, \Delta)$ is the radiation pattern. $C(\omega, \phi, \Delta)$ is the effect of the path along the core-mantle boundary on the waves. $M_d(\omega, \phi)$ and $M_u(\omega, \phi)$ represent, respectively, the effects of the downward and upward paths through the mid-mantle on the waves. $U(\omega)$ is the impulse response of the crust and uppermost mantle under the station. This formulation is slightly different from Mula's (1981) since he used the term $K(\omega)$ and accounted solely for crustal effects. We have allowed for the possibility that the upper mantle sustains significant heterogeneities. Lastly, $I(\omega)$ is the instrument response.

Assuming that the amplitudes along the core-mantle boundary decay exponentially with distance (Phinney and Alexander, 1966; Chapman and Phinney, 1972; Van Loenen, 1988; Aki and Richards, p. 457, 2002) and that the dependence on the azimuth will be averaged for a small enough azimuthal window (less than 20°), let

$$C(\omega, \varphi, \Delta) = e^{-\gamma(\omega)\Delta} \sin^{-1/2} \Delta, \tag{2}$$

where $\sin^{-1/2} \Delta$ is the geometrical spreading factor. The term $\gamma(\omega)$ is the decay constant. Anelastic attenuation has the effect of reducing wave

amplitudes. Valenzuela-Wong (1996) carried out tests to evaluate the relative contributions of anelastic attenuation versus velocity structure on the decay constant. He concluded that the amplitude decay due to the diffraction process is clearly more significant than the decay due to anelastic attenuation.

It is possible to solve for the decay constant by obtaining the spectral amplitude ratio of any station j relative to a reference station r. Upon division, the term $S(\omega)$ cancels out because we have assumed no directivity effects, and because we chose a narrow azimuthal window. The term $M_d(\omega, \phi)$ also cancels out upon division because the downgoing path is approximately the same for all stations since a narrow azimuthal window was used; we further consider the mid-mantle to be nearly homogeneous. The term $M_u(\omega, \phi)$ is not considered significant on the premise of mid-mantle homogeneity. Under the previous assumptions, the spectral division takes on the following form:

$$\frac{A_j(\omega)}{A_r(\omega)} = \frac{R_j(\varphi, \Delta)\ e^{-\gamma(\omega)\Delta_j}\ \sin^{-1/2}\ \Delta_j\ U_j(\omega)\ I_j(\omega)}{R_r(\varphi, \Delta)\ e^{-\gamma(\omega)\Delta_r}\ \sin^{-1/2}\ \Delta_r\ U_r(\omega)\ I_r(\omega)}$$
(3)

Solving for the decay constant, $\gamma(\omega)$, yields

$$\ln \left\{ \frac{A_j(\omega)\ R_r(\varphi, \Delta)\ U_r(\omega)\ I_r(\omega)\ \sin^{1/2}\ \Delta_j}{A_r(\omega)\ R_j(\varphi, \Delta)\ U_j(\omega)\ I_j(\omega)\ \sin^{1/2}\ \Delta_r} \right\} = \gamma(\omega)\left[\Delta_r - \Delta_j\right]$$
(4)

The terms A_j and A_r are the recorded seismograms; R_j and R_r can be calculated from the focal mechanisms, readily available in the literature; and I_j and I_r are the instrument responses, known from manufacturer's specifications or empirically determined. Finally, based on earlier literature, Mula (1981) set the ratio K_j/K_r, for crustal effects, equal to 1. Valenzuela-Wong (1996) showed a procedure to obtain the ratio U_j/U_r using data from other earthquakes (at shorter epicentral distances) recorded by the same stations. Additionally, he also explored the effect of setting the ratio $U_j/U_r = 1$. Valenzuela-Wong (1996) could not fit the observed decay constant when he applied crustal and upper mantle corrections. He speculated that the crustal and upper mantle effects are too small and thus applying the corrections would adversely affect the measurement of the decay constant. Alternatively, if the quality of the data he used to evaluate the corrections was not good enough, then the measurement of the decay constant would have been degraded. In this paper the decay constant was determined assuming that $U_j/U_r = 1$.

Data and procedure

Data from the Tonga Islands earthquake of April 7, 1995 was analyzed to determine the radial velocity structure of the D" region under the east central Pacific Ocean, in a spot centered at 19°N, 132°W (Figure 1). The event parameters are as follows. 22:06:57 UT, 15.20°S, 173.53°W, depth 40 km, M_w=7.3, M_o=1.3×10²⁰ N m, ϕ=165°, δ=18°, λ=159°. The origin time, latitude, and longitude were taken from the National Earthquake Information Center (NEIC) catalog. The moment magnitude and the seismic moment were taken from the Harvard University Centroid Moment Tensor (CMT) catalog (Dziewonski *et al.,* 1996). The event depth as well the nodal plane parameters were constrained through waveform modeling. Reflectivity synthetic seismograms were generated using a technique similar to the one described by Kennett (1980). The source was placed at different depths in order to fit the arrival times of the S and sS waves at the shortest distances, and the S_{diff} and sS_{diff} arrivals later in the profile (Figures 2 and 3). The nodal plane was constrained by keeping the dip and slip taken from the Harvard CMT catalog (Dziewonski *et al.,* 1996) fixed while varying the strike in 5° steps and looking for the best fit to the relative amplitudes between the S and sS (or between S_{diff} and sS_{diff}) phases. Additionally, the source time function (STF) was determined and a double rupture was found for this earthquake. The source time function was convolved with the synthetics to obtain the best fit to the data. This STF is made up of two overlapping trapezoids which amount to a total duration of 23 s. The first trapezoid has the largest amplitude. The amplitude of the second trapezoid is roughly two thirds the amplitude of the first one. The seismograms used were recorded at the temporary stations of the Missouri to Massachusetts (MOMA) broadband array (Wysession *et al.,* 1996; Fischer *et al.,* 1996). The seismometers were provided by the Incorporated Research Institutions for Seismology (IRIS) Program for Array Seismic Studies of the Continental Lithosphere (PASSCAL). Both Streckeisen STS-2 and Güralp CMG3-T broadband seismometers were used. Their amplitude responses in velocity are essentially the same. The amplitude response is flat in the frequency range from 0.0083 to 50 Hz (periods between 120 and 0.02 s). Figure 1 shows the epicenter, the stations, and the region of D" sampled under the east central Pacific. At the epicentral distances involved, between 94° and 108°, both S and S_{diff} arrivals are observed, as shown in Figure 2 and 3. The profile spans a distance at the core-mantle boundary of 14° and the azimuthal window is extremely narrow, only ~1°, thus providing a very coherent and stable sampling of the base of the mantle. The scale of the region sampled is on the order of 900 km.
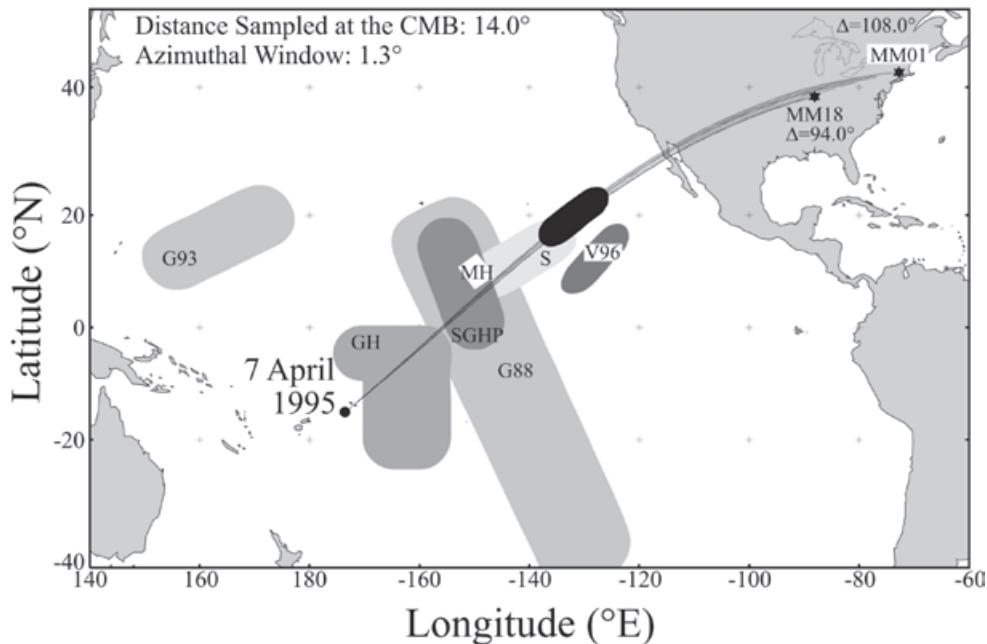
Figure 1. Ray paths of *SH* and *SH*diff waves from the Tonga earthquake of 7 April 1995 recorded by the Missouri to Massachusetts (MOMA) broadband array in the northeastern United States. The dot marks the epicenter. Stations MM01 and MM18 served as anchors for the MOMA array. The lowermost mantle is sampled under the east central Pacific Ocean as indicated by the black area along the ray paths. As the epicentral distances vary between 94° and 108°, the farthest arrivals are fully diffracted waves while the nearest ones are direct waves traveling within D". The distance sampled at the core-mantle boundary (CMB) is 14°. The azimuthal window is ∼1.4°, providing a very coherent and stable sampling of the CMB. Also shown are the locations of previous studies of D" under the Pacific. The codes stand for the following work. S: Schlittenhardt *et al.* (1985); G88: Garnero *et al.* (1988); G93 and SGHP: Garnero *et al.* (1993); MH: Mori and Helmberger (1995); GH: Garnero and Helmberger (1995, 1996); V96: Valenzuela-Wong (1996), and Valenzuela and Wysession (1998). For discussion refer to Section 5.1.

The steps followed to determine the decay constant using data from the MOMA array are described below. Figure 3 shows the instrument-deconvolved, displacement waveforms as recorded in the transverse components. The amplitude spectrum for each station was obtained from a 70 s time window containing both the *SH*diff and the *sSH*diff pulses (or *SH* and *sSH,* depending on the actual distance). Records were bandpass filtered to retain frequencies between 0.005 and 0.500 Hz (i. e., 200 to 2 s period). Figure 4 shows the amplitude spectra at all the stations that recorded this event. The vertical dashed lines bound the frequency range (from 0.014 to 0.043 Hz, or alternatively periods from 71 to 23 s) where the decay constant can be reliably determined following a criterion which will be explained below. The amplitudes are largest within this frequency band, thus providing the best signal-to-noise ratio (SNR). Also noticeable in
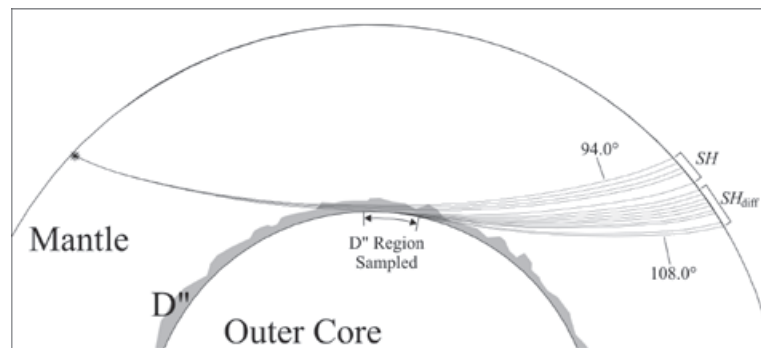

Figure 2. Cross section showing the region of the core-mantle boundary sampled by the Tonga earthquake of 7 April 1995 recorded by the MOMA array in the northeastern United States. The ray paths are also shown. At these epicentral distances, between 94° and 108°, both *SH* and *SH*diff waves were recorded.
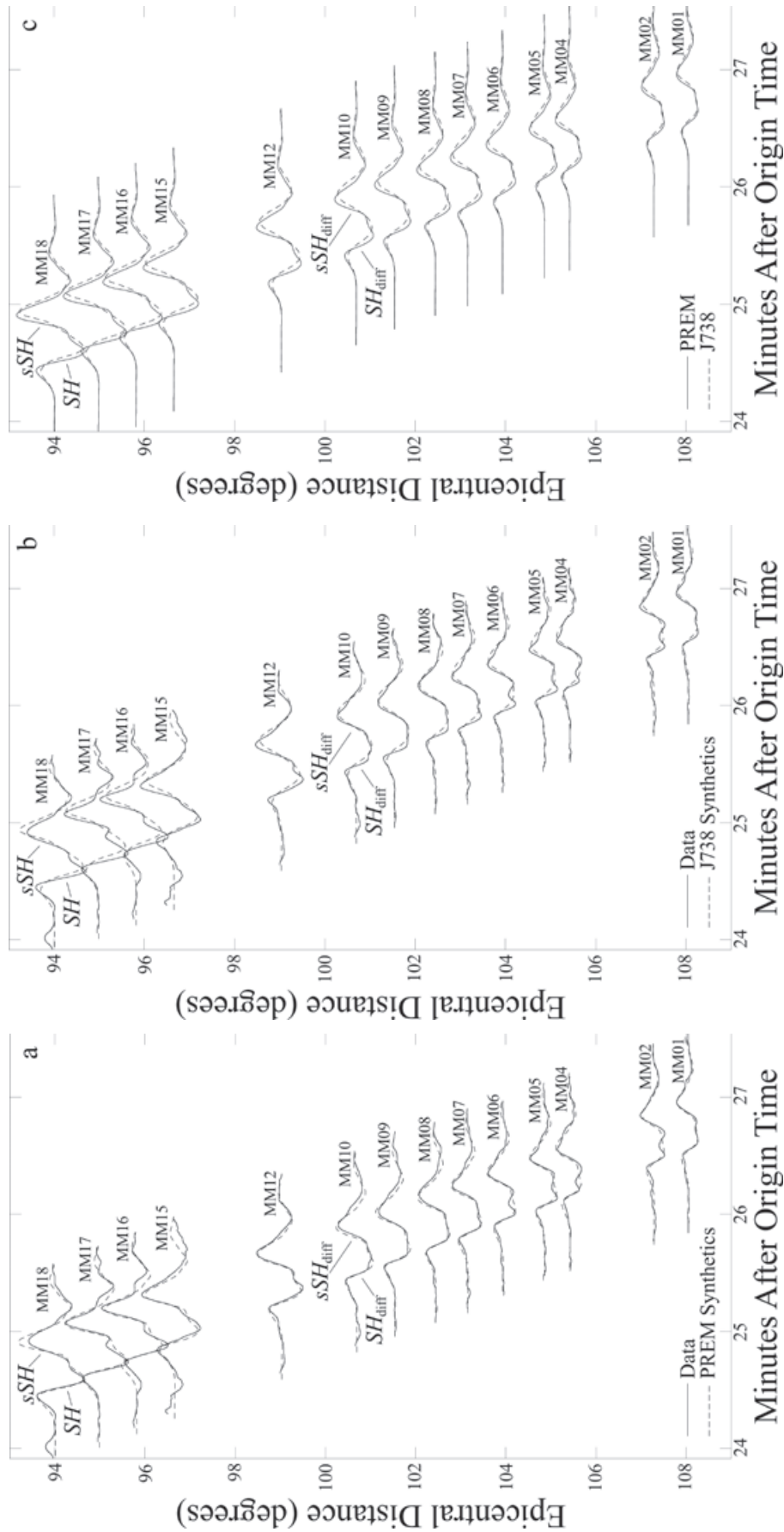
Figure 3. Instrument-deconvolved, displacement, transverse records from the Tonga earthquake of April 7, 1995 recorded by the MOMA array. Records were bandpass filtered between 200 and 2 s (between 0.005 and 0.500 Hz). Synthetic waveforms correspond to models (a) PREM and (b) J738. The synthetics were normalized to match the amplitude of the observed pulses. The depth of the earthquake was constrained through waveform modeling of the surface reflected phases sSH and sSH_{diff}. A source time function with a double rupture was applied. (c) compares PREM to J738 synthetics at the same scale.

Figure 4 is the expected decrease in amplitude with increasing epicentral distance (Phinney and Alexander, 1966; Chapman and Phinney, 1972; Van Loenen, 1988; Aki and Richards, p. 457, 2002). In general the amplitudes (Figure 4) drop to a low at a frequency of 0.05 Hz and are highly variable from station to station at higher frequencies. Figure 5 shows the logarithmic amplitude ratio for each station, relative to the nearest station (MM18) chosen as the reference, plotted as a function of distance at a frequency of 0.0297 Hz (period = 33.7 s). The decay constant is the slope of a straight line, obtained through a least squares fit. At this frequency $\gamma = 0.079$ and the correlation coefficient for the fit is r = 0.980. Given that the decay constant is the slope calculated at a certain frequency, it is expected that γ will take different values at different frequencies, as shown in Figure 6 for selected frequencies. A plot of the decay constant, as well as the corresponding correlation coefficient, as a function of frequency is presented in Figure 7. It is necessary to stress the importance of determining the correlation coefficient for the linear fit. In order for a measurement of the decay constant to be considered reliable, a correlation coefficient greater than or equal to 0.9 was required. The square of the correlation coefficient is a measure of how much one variable Y can be accounted for through a linear relationship as a function of the variable X (Walpole and Myers, pp. 403-409, 1993). Thus, using the customary value of r ≥ 0.9, X accounts for $r^2 \geq 0.81$ (81%) of the values in Y through a linear relationship. The same requirement was imposed on decay constants determined by forward modeling as described in the next section. In this paper the

requirement that r ≥ 0.9 was used more as a measure to determine if the variables could be appropriately related by the decay constant, i. e., that it was appropriate to fit the data through a straight line (Walpole and Myers, pp. 403-409, 1993), than as a measure of data scatter about a straight line. At certain frequencies r < 0.9 and, unlike Figure 5, deviations from a straight line were observed (e. g., sigmoidal or arc-shaped curves, or a decreasing trend followed by a sudden increase). This meant the breakdown of the assumption that the decay constant is a good model for the amplitude decay, and furthermore that Equation (4) was not valid at these frequencies. This effect was especially obvious for decay constants determined from forward models. To a large extent, reliable values of the correlation coefficient (r ≥ 0.9) were used to determine the range of frequencies where the measurement of the decay constant was valid. In Figure 7, as well as in Figure 4, this range goes from 0.014 to 0.043 Hz. In general γ shows an increasing trend with increasing frequency, except at the highest frequencies (from 0.038 to 0.043 Hz) where a slight drop occurs (Figure 7). Figure 8 shows the measured decay constant and the 1-σ standard deviation obtained from the least squares fit. For comparison purposes Figure 8 also shows the decay constant observed in nearby region V96 (see Figure 1) where a discontinuity at the top of D" was previously reported (Valenzuela-Wong, 1996; Valenzuela and Wysession, 1998). The two decay constants show some overlap at low and high frequencies. They clearly differ, however, in the range from 0.018 to 0.031 Hz.
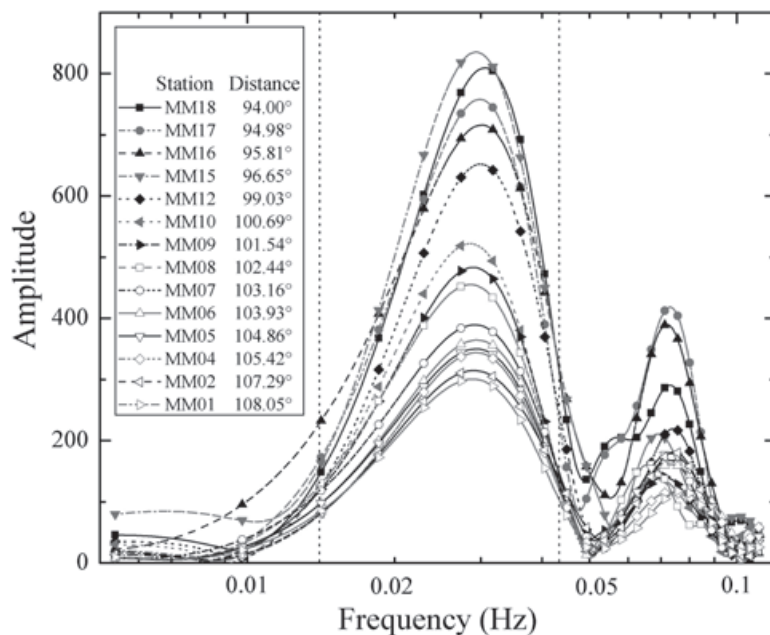

Station	Distance
MM18	94.00°
MM17	94.98°
MM16	95.81°
MM15	96.65°
MM12	99.03°
MM10	100.69°
MM09	101.54°
MM08	102.44°
MM07	103.16°
MM06	103.93°
MM05	104.86°
MM04	105.42°
MM02	107.29°
MM01	108.05°

Figure 4. Amplitude spectra for the Tonga earthquake of 7 April 1995 recorded by the MOMA array. Notice the decay of the amplitude as distance increases. Records were bandpass filtered between 200 and 2 s (between 0.005 and 0.500 Hz). *SH* waves at these distances have most of their energy at periods between 71 and 23 s (between 0.014 and 0.043 Hz) as indicated by the vertical dashed lines.

Figure 5. Logarithmic amplitude ratio for each station, relative to reference station MM18, plotted as a function of distance. The frequency is 0.0297 Hz (33.7 s period). The decay constant is the slope of the straight line, obtained through a least squares fit. The decay constant is γ =0.079 and the corresponding correlation coefficient is r=0.980.
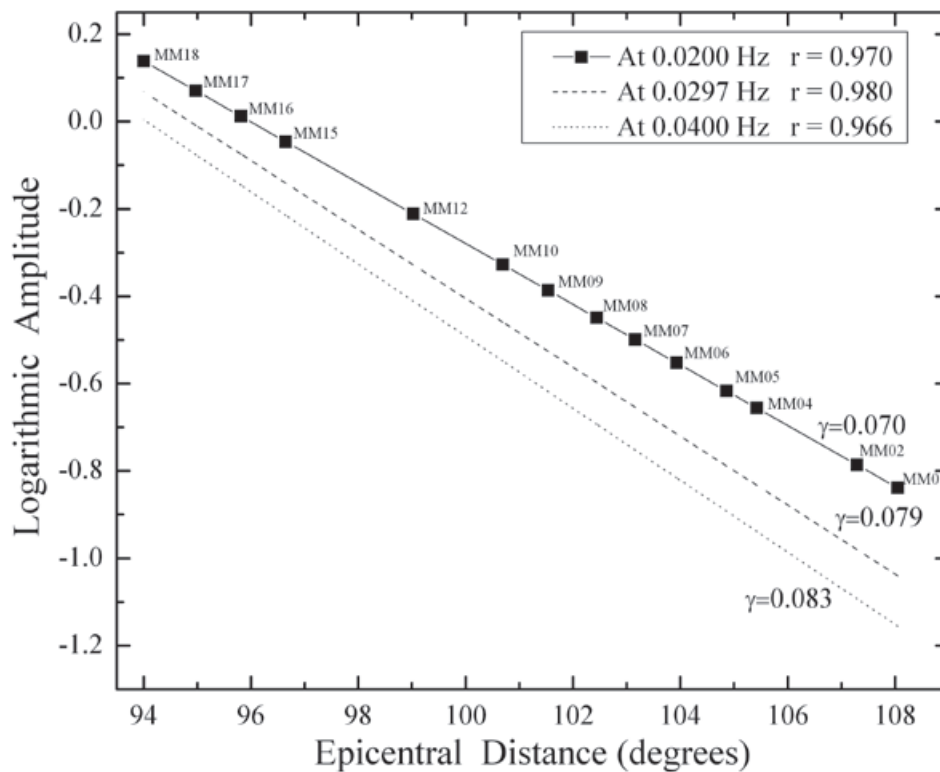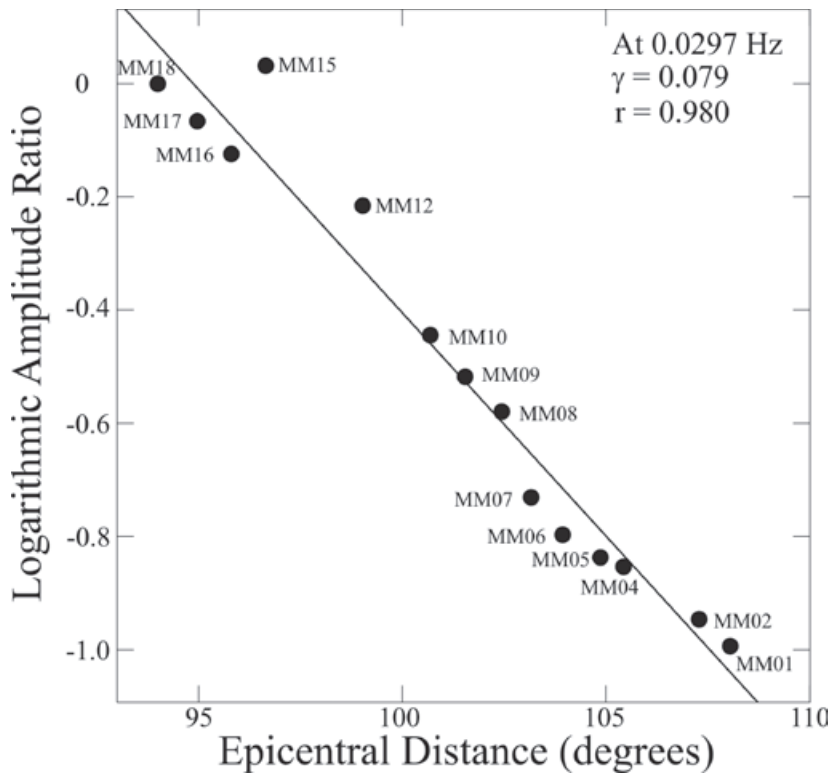
Figure 6. Decay constant obtained as in Figure 5 shown at selected frequencies. The value for γ is different at different frequencies. Squares are not actual data points, they are only intended to show the epicentral distance for each station.
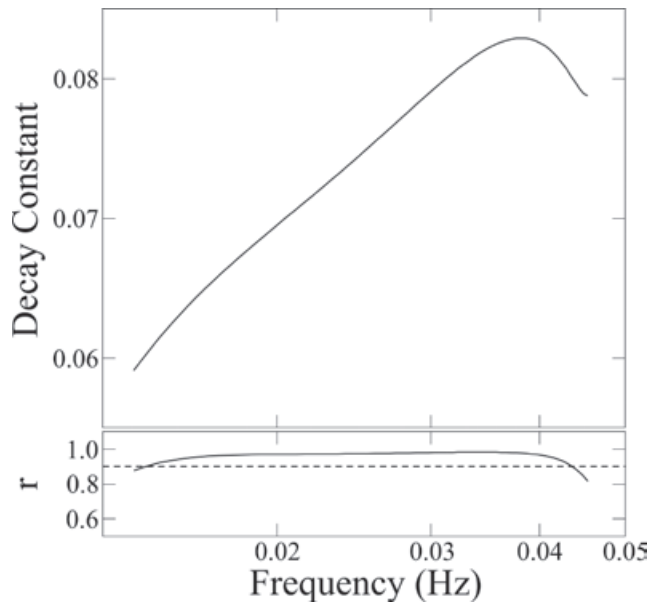
Figure 7. Decay constant plotted as a function of frequency. Also shown is the correlation coefficient for the least squares fit. Decay constants are considered reliable if their correlation coefficients are equal to or greater than 0.9, as indicated by the horizontal dashed line.

data (Bolt *et al.,* 1970; Doornbos and Mondt, 1979b; Mula, 1981; Doornbos, 1983; Doornbos *et al.,* 1986). Nonetheless, the reliability of the method has been firmly established (Bolt *et al.,* 1970; Doornbos and Mondt, 1979b; Mula, 1981; Doornbos, 1983; Doornbos *et al.,* 1986; Van Loenen, 1988; Valenzuela-Wong, 1996; Valenzuela and Wysession, 1998). Given the uneven distribution of sources and receivers around the world, the use of diffracted waves makes it possible to increase the coverage of D″ afforded by other seismic phases (Wysession, 1996a).

Results

In order to determine the radial velocity structure at the base of the mantle, reflectivity synthetic seismograms were generated by forward modeling while trying a set of proposed models. The algorithm used to generate synthetic seismograms was provided by Tim Clarke and is similar to the one described by Kennett (1980). Three criteria were followed to guarantee the reliability of the best-fitting models. First, a good fit of the modeled decay constant to the observations was sought. Second, the correlation coefficient of the least squares fit to a straight line (decay constant) had to be greater than or equal to 0.9. Third, synthetic and recorded time domain waveforms were compared in order to avoid features which do not correspond with the observations.

Models were organized into the following groups and their effects on the decay constant were explored. (*a*) The Preliminary Reference Earth Model, PREM, (Dziewonski and Anderson, 1981), models with (*b*) a gradual decrease of the velocity throughout D″ with increasing depth, (*c*) a gradual increase, and (*d*) a discontinuous increase in the velocity followed by a gradual decrease. Special attention was given to discontinuous models in order to determine the response of the decay constant to changes in (*i*) the amount of the velocity decrease throughout D″, (*ii*) the thicknes of D″, (*iii*) the velocity increase at the discontinuity, and (*iv*) the velocity gradient above D″. Earlier work has shown the importance and prevalence of velocity models with a discontinuity at the top of D″ (e. g., Lay and Helmberger, 1983; Nataf and Houard, 1993; Krüger *et al.,* 1995; Loper and Lay, 1995; Wysession *et al.,* 1998; Helmberger

The range of frequencies chosen to analyze the decay constant is controlled by the energy content of the diffracted waves. At higher frequencies the effect of scattering is important (Bataille and Flatté, 1988; Bataille *et al.,* 1990; Bataille and Lund, 1996; Stein and Wysession, pp. 168-169, 2003) and consequently diffracted waves have little energy. This makes it impossible to fit the data with the decay constant. At lower frequencies, as the diffracted wave travels farther along the CMB it becomes increasingly depleted in high frequency energy given that the diffraction process is more efficient at low frequencies (Aki and Richards, p. 457, 2002; Stein and Wysession, p. 74, 2003). In this regard the frequency content, between 0.014 and 0.043 Hz (periods between 71 and 23 s), observed in this study for the *SH* wave (at distances between 94° and 108°) agrees with earlier work using diffracted waves (Bolt *et al.,* 1970; Doornbos and Mondt, 1979b; Mula, 1981; Doornbos, 1983; Doornbos *et al.,* 1986; Valenzuela-Wong, 1996; Valenzuela and Wysession, 1998). The third effect controlling the frequency content is the radial velocity structure at the base of the mantle (Mula, 1981; van Loenen, 1988; Valenzuela-Wong, 1996; Valenzuela and Wysession, 1998) and is in fact the reason that the decay constant technique was chosen for this study. In the analysis described herein, the effects of both the diffraction process and the radial velocity structure are accounted for by the forward modeling of reflectivity synthetic seismograms. The resolution of the decay constant method is limited to long wavelength structures (~1000 km) because of the low frequency nature of diffracted waves. This fact has long been known and researchers have been careful not to overinterpret their
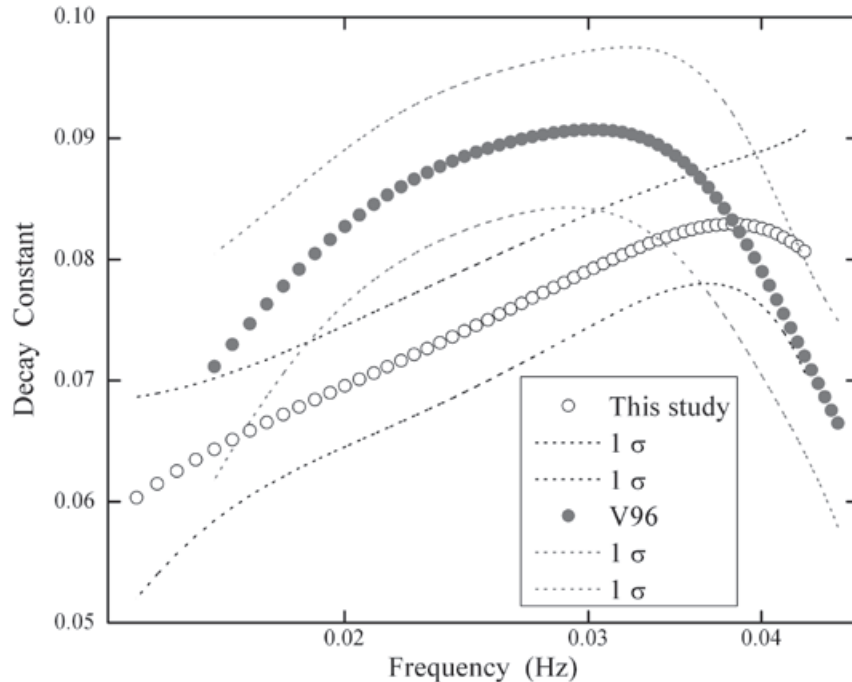
Figure 8. Comparison of the decay constant measured in this study (black, open circles) with the decay constant observed in nearby region V96 (gray, solid circles) as shown in Figure 1. The dashed lines represent one standard deviation for the two measurements. A discontinuity at the top of D" has been reported in region V96 (Valenzuela-Wong, 1996; Valenzuela and Wysession, 1998). These decay constants overlap somewhat at the low and high frequency ends, but are clearly different at intermediate frequencies.

et al., 2005; and Lay and Garnero, 2007, 2011). Figure 1 shows locations where the discontinuity has been found under the Pacific Ocean (G88 from Garnero *et al.,* 1988; SGHP and G93 from Garnero *et al.,* 1993). In particular, Valenzuela-Wong (1996) and Valenzuela and Wysession (1998) found that a model with a discontinuous increase in the velocity followed by a gradual decrease (RJK2705) best fits the decay constant in a region of D" located near and to the southeast of the one reported in this study (V96 in Figure 1). In that case the decay constant from PREM is clearly different than that of RJK2705's and does not match the observations at all. Based on the preceding results it was expected that models with a discontinuity at the top of D" would provide the best fit to the observations. It was indeed possible to fit the data using discontinuous model J738, but as it will be shown, model PREM provided an even better fit to the decay constant and the waveforms. Given that both the diffraction process and anelastic attenuation lead to the amplitude decrease of seismic waves, Valenzuela-Wong (1996) and Valenzuela and Wysession (1998) calculated the decay constant by varying the value of Q, the seismic quality factor, in their models in order to evaluate the relative contribution of the two processes. In this study PREM provided a good fit to the data, therefore trying different values of Q was not deemed necessary. Furthermore, Valenzuela-Wong (1996) concluded that even

for models with a discontinuity, increasing Q_μ above 156 has only a small effect on the decay constant. Most of the models available in the literature have values for Q_μ in D" greater than 200 (Anderson and Hart, 1978a, 1978b; Sailor and Dziewonski, 1978; Stein *et al.,* 1981; Dziewonski and Anderson, 1981; Widmer *et al.,* 1991; Bhattacharyya *et al.,* 1995a, 1995b; Durek and Ekström, 1996). For example $Q_\mu = 312$ in PREM.

Four different models were initially tested and are shown in Figure 9a. The Preliminary Reference Earth Model (PREM), proposed by Dziewonski and Anderson (1981), was the first one evaluated. It is a global, homogeneous, and one-dimensional model of the seismic velocities, density, and anelastic attenuation as a function of depth. In order to create the model, different kinds of data such as body waves, long period surface waves, and free oscillations were taken into account. The *S* wave velocity in PREM is shown by the dash-dotted line in Figure 9a. It has a gradual velocity increase with increasing depth throughout most of the lower mantle and a very slight decrease throughout a 150 km-thick D". Models A, B, and C are variations of PREM in the lowermost 150 km of the mantle, i. e. the D" region. Model A shows a gradual decrease in the velocity from top to bottom of D", model B shows a gradual increase, and model C shows a sudden increase at the top of D" followed by a constant velocity all the way down to the bottom of D".
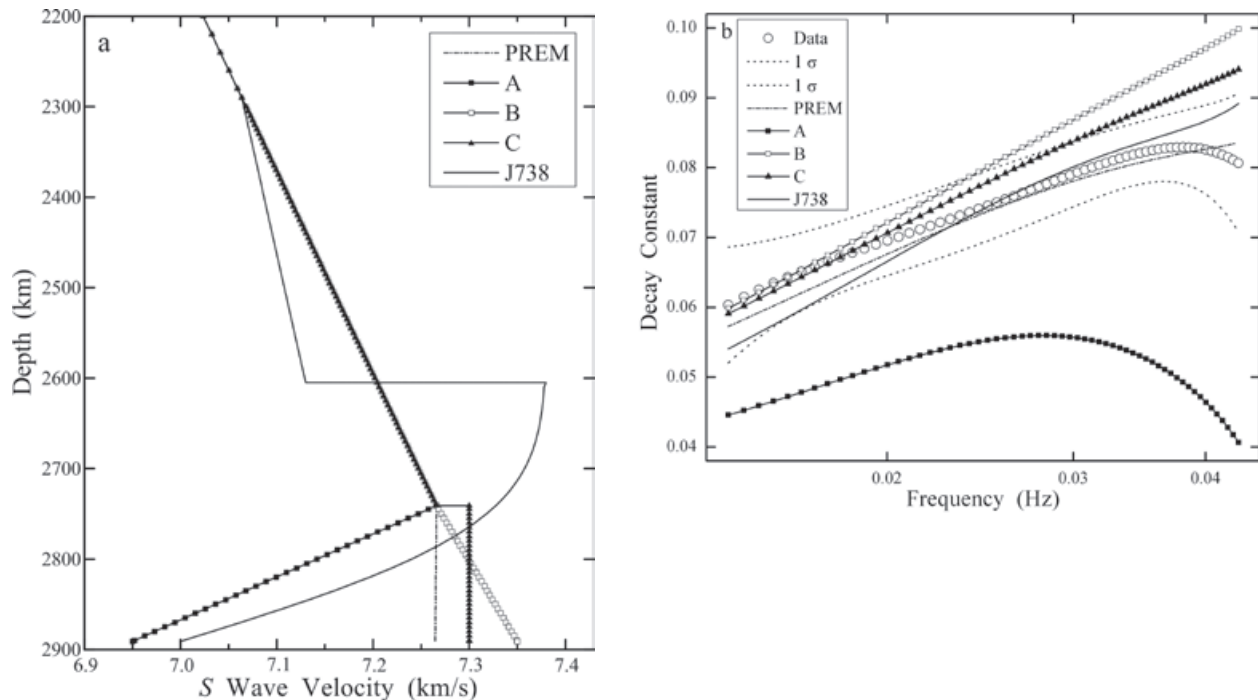
Figure 9. (a) Models of lowermost mantle shear velocity structure. Dot-dashed line is for model PREM. It has a very slight velocity decrease with increasing depth throughout a 150 km-thick D″. There is no discontinuity at the top of D″. Models A, B and C are variations of PREM in the bottom 150 km. Model A shows a gradually decreasing velocity. Model B, a gradually increasing velocity. Model C, a discontinuous increase at the top of D″ followed by a constant velocity down to the CMB. Model J738 is only shown for comparison and will be discussed later. (b) Decay constants obtained from the corresponding models. The open circles show the data and the dashed lines represent one standard deviation. PREM fits the data as it falls within the error bars. The decay constant from model A is too low to fit the data. Model B matches the observations only at low frequencies, and so does model C for a somewhat broader frequency range.

In order to generate reflectivity synthetic seismograms, models for the compressional velocity, the density, and the bulk and shear seismic quality factors were specified in addition to the shear velocity model. The same percentage change in P velocity models was used as for S velocity models. Since changes in seismic wave velocity can be caused by thermal (Stacey and Loper, 1983; Lay and Helmberger, 1983; Doornbos *et al.,* 1986; Lay, 1989; Loper and Lay, 1995; Wysession *et al.,* 1998; Lay *et al.,* 1998; Garnero, 2000) or chemical (Lay and Helmberger, 1983; Lay, 1989; Loper and Lay, 1995) heterogenities at the base of the mantle, Valenzuela-Wong (1996) tested different density models consistent with both possibilities. He found that the differences caused by the different density models on the decay constant are relatively small, in agreement with earlier work by Doornbos and Mondt (1979a). Therefore, for simplicity all modeling in this paper was done using thermal density models alone. In this way, a velocity increase is correlated with a density increase, and likewise a velocity drop

is correlated with lowered densities. The seismic quality factors, Q_K and Q_μ, used for the models of D″ in this work were taken from PREM. The models for P and S velocities, density, and Q used in the generation of reflectivity synthetic seismograms are identical to PREM through the crust and the mantle down to 2,300 km depth, and also in the core.

The fits of the synthetic to the observed decay constant are shown in Figure 9b for models PREM, A, B, and C. The dashed lines represent the 1-σ standard deviation for the measured decay constant as obtained from the least squares fit. The decay constant from model A is clearly too low to match the observations. Model B fits the measured decay constant at low frequencies, from 0.014 to 0.023 Hz, whereas model C can fit the data up to frequencies as high as 0.030 Hz. PREM fits the data well because its decay constant falls within the error bars for the data throughout the entire frequency range from 0.014 to 0.043 Hz. Valenzuela-Wong (1996) and Valenzuela and Wysession (1998) found that

certain models with a discontinuous increase in the velocity followed by a gradual decrease with increasing depth best fit the decay constant in a region of D" near the area of this study (V96 in Figure 1) and also for D" under easternmost Siberia. Simple models such as PREM, A, or B, or variations of these models, however, could not fit their data. So, next we tried to fit our data using models that have a sudden increase in the velocity followed by a gradual decrease. Some examples are given below.

Figure 10 shows the effect of changing the velocity at the CMB while keeping constant the velocity jump at the discontinuity. Models F02, G02, and H all have a discontinuous *S* wave velocity increase at the top of D" from 7.13 to 7.34 km/s (Figure 10a). Next the velocity undergoes a gradual decrease down to the CMB in the form of a complementary error function. The choice of a complementary error function is consistent with the perception of D" as a thermal boundary layer (Stacey and Loper, 1983; Lay and Helmberger, 1983; Doornbos *et al.,* 1986; Lay, 1989; Loper and Lay, 1995; Wysession *et al.,* 1998; Lay *et al.,* 1998; Garnero, 2000; Lay and Garnero, 2011). The complementary error function is used to describe the temperature as heat is transferred by conduction through a

thermal boundary layer (Turcotte and Schubert, pp. 153-157, 2002). Both the velocity and density profiles are assumed to depend on the temperature and thus follow a complementary error function within the thermal boundary layer (TBL). The thickness of the basal layer is 286 km. Models F02, G02, and H illustrate the effect of decreasing the velocity at the CMB (Figure 10a). These velocities are 7.19, 7.00, and 6.90 km/s, respectively. The corresponding decay constants are shown in Figure 10b. The decay constant from model F02 fits the data at low frequencies, from 0.014 to 0.019 Hz, but it is too high at higher frequencies. Model G02 does a good job at large frequencies, from 0.020 to 0.043 Hz, but it fails to fit the data at lower frequencies. Lastly, the decay constant from model H is too low throughout the entire frequency range.

Models of the J series explore the effect of varying the velocity increase at the discontinuity (at the top of D"). Figure 11a shows models J724, J734 (which is the same as G02), J738, and J744. The number after the J corresponds to the increased *S* wave velocity at the discontinuity: 7.24, 7.34, 7.38, and 7.44 km/s, respectively. Therefore the velocity jump at the discontinuity is 1.54, 2.95, 3.51, and 4.35 % for models J724, J734, J738, and J744, respectively. The starting
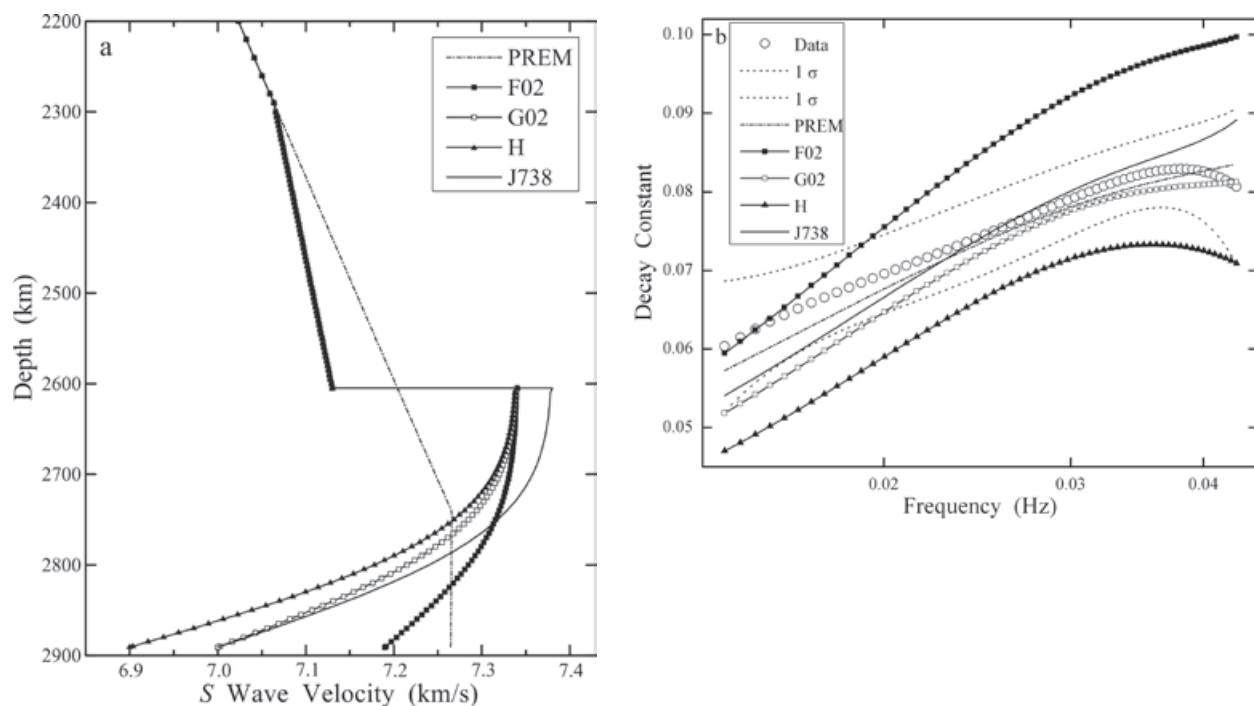

Figure 10. Determining the effect of varying the velocity at the core-mantle boundary. (a) Shown here are models F02, G02 and H in order of decreasing velocity at the CMB. All models use a complementary error function to describe the velocity decrease throughout the lowermost mantle. Model J738 will be discussed later. (b) Corresponding decay constants. Notice the decreasing decay constant with decreasing velocity at the CMB. None of these models fit the observations throughout the entire frequency range.

velocity at the discontinuity is 7.13 km/s. The velocity at the CMB is 7.00 km/s and the basal layer thickness is 286 km. Figure 11b shows the decay constants. These follow a straightforward pattern. Larger velocity jumps are associated with larger decay constants. The decay constant from model J724 is clearly too low to fit the data. Model J734 works well only at high frequencies, from 0.020 to 0.043 Hz. Model J738 does a good job at all frequencies. Model J744 fits the observations at low frequencies, from 0.014 to 0.025 Hz, but breaks down at higher frequencies.

In other models (not shown) the thickness of D" and the velocity gradient above D" were changed in order to evaluate their effect on the decay constant. These could not match the observations. Out of a total of 29 different models tested, two fit the data given that their decay constants fall within the error bars for the data. These are PREM and J738 (Figure 11). PREM, however, provides a better fit because its decay constant is closer to the observed decay constant for most frequencies (Figure 11b). The time domain waveforms from PREM are compared to the observations in Figure 3a and also show a good fit. The SH_{diff} (or SH) pulse from the J738 synthetics shows a poorer fit to the data as it is too narrow, especially in the distance range from

99° to 106° (Figure 3b). The PREM and J738 synthetic waveforms are compared in Figure 3c. PREM is our preferred model given that it provides a better fit than J738 in both the time and frequency domains.

Discussion

Under this region of the east central Pacific Ocean PREM implies that D" is 150 km thick and that the S wave velocity gradient is slightly negative throughout. No discontinuity is observed at the top of D". The observation of a PREM velocity structure is consistent with a thermal boundary layer because the velocity gradient is decreased relative to the rest of the lower mantle. Due to its silicate composition, the mantle has a low thermal conductivity and a high viscosity (Loper and Lay, 1995) and is thus expected to act as a TBL. The temperature increases with increasing depth while the seismic velocity gradient drops. A PREM structure is also consistent with chemical reactions between mantle and core materials which could lead to iron enrichment of the silicates in D" (Knittle and Jeanloz, 1989, 1991). The denser, iron-enriched silicates would accumulate in the lowermost mantle and are seismically slow (Williams and Garnero, 1996; Wysession et al., 1998), which is consistent with the reduced S
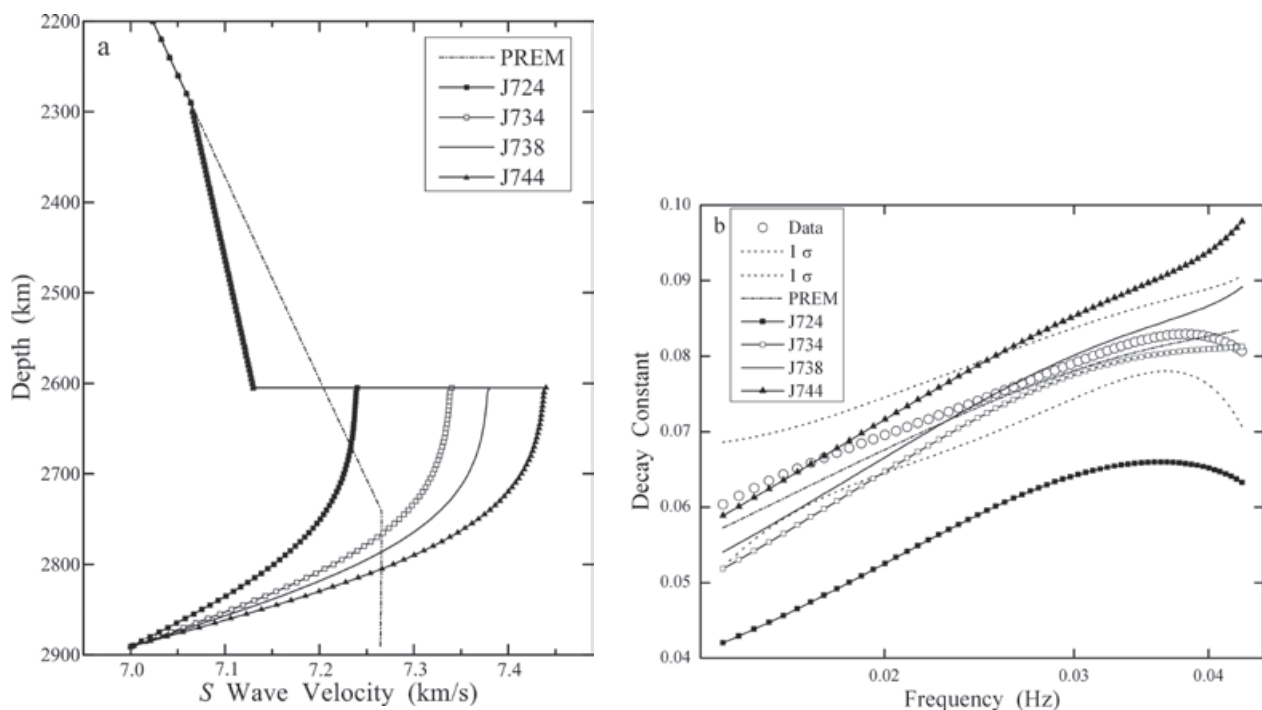

Figure 11. Effect of the velocity increase at the discontinuity. (a) Models of the J series in order of increasing jump in the velocity. D" thickness is 286 km. The velocity jump at the discontinuity varies between 1.54 and 4.35 %. (b) Corresponding decay constants. Model J738 fits the data as it falls within the error bars. PREM, however, stays closer to the observed decay constant at most frequencies and is thus considered a better model. Also see the fits to the time domain waveforms for these two models in Fig. 3.

wave velocity gradient observed in PREM. The accumulation of subducted slabs at the base of the mantle is expected to produce increased seismic velocities (Wysession, 1996b) and is thus associated with the seismic discontinuity. Given that no subduction has taken place at this location of the Pacific in the past 180 Myr (Richards and Engebretson, 1992; Ricard et al., 1993; Lithgow-Bertelloni and Richards, 1998) no discontinuity would be expected, in agreement with a PREM structure. Hernlund et al. (2005) proposed that a hot profile through the mantle, such as in a mantle upwelling, would remain within the perovskite stability field because its geotherm would not intersect the post-perovskite phase boundary. This mechanism is suggested as an explanation for the absence of the discontinuity. In this location of D" under the east central Pacific, the temperature is not as high as in the large low-velocity province (LLVP) beneath the Pacific found to the southwest and does not appear to be consistent with the model of Hernlund et al. (2005).

Comparison with the radial velocity structure of D" under the Pacific Ocean

A velocity discontinuity at the top of D" has been observed in many different regions around the world; see Nataf and Houard (1993); Krüger et al. (1995); Loper and Lay (1995); Wysession et al. (1998); Helmberger et al. (2005); Lay and Garnero (2007, 2011); Garnero and McNamara (2008); and Wookey and Dobson (2008) for a review. Nonetheless, there exist regions where the discontinuity has not been found (e. g., Wysession et al., 1998). Studies using the prevalent method for determining the radial velocity structure of the lowermost mantle, i. e. the search for the triplicated *Scd* arrival (e. g., Lay and Helmberger, 1983), argue for the existence of a strong discontinuity at the top of D" in regions of downwelling mantle and high shear velocities in tomographic models (Helmberger et al., 2005). Assuming that a solid-solid phase transition in the lowermost mantle were to occur, Sidorin et al. (1999a, 1999b) developed a method to thermally map shear wave velocities into temperatures and from there to the elevation of a phase/seismic velocity discontinuity above the CMB. Under this model, the discontinuity would be a global feature and it would be found higher above the CMB in regions of high velocities, and closer to the CMB where velocities are low. The experimental observation of a phase transition from perovskite to post-perovskite at 125 GPa (equivalent to 2,700 km depth) and 2,500 K (Murakami et al., 2004) seems generally consistent with seismic observations of the velocity discontinuity at the top of D". The evidence for a D" triplication from secondary arrivals between *S* and *ScS,* however,

is less convincing in regions of low velocities and possible upwelling such as under the central Pacific (Helmberger et al., 2005). Newer results, using expanded data sets, as well as a stacking technique to improve the observation of the *SdS* phase, confirm the existence of the discontinuity in certain regions under the central Pacific (Russell et al., 2001; Avants et al., 2006; Lay et al., 2006; and Ohta et al., 2008).

One of the earliest studies that specifically searched for a discontinuity and failed to find it was conducted by Schlittenhardt et al. (1985). Amongst others, they used earthquakes in Fiji, recorded by stations in North America, which sampled a patch of D" to the southwest of, and partially overlapping, the region chosen for this study (their study area is labeled S in Figure 1). They looked for, but did not find, the waveform distortions of P_{diff} and SH_{diff} pulses produced by a triplicated arrival at epicentral distances between 95° and 120°. Schlittenhardt et al. (1985) generated reflectivity synthetic seismograms comparing PREM to discontinuous model SLHO (Lay and Helmberger, 1983) and concluded that PREM fits better the time domain waveforms. In the present study, PREM was chosen as the preferred model because it fits both the decay constant (in the frequency domain) and the SH_{diff} waveforms (in the time domain). Garnero et al. (1988) proposed a lower mantle model whereby a V_S discontinuity (model B) in regions of the Pacific bordering the coast of North America fades away to no discontinuity (model A) in the mid-Pacific (G88, Figure 1). They based their conclusions on anomalously large *S-SKS* times and on the lack of waveform evidence at 92° for any arrivals from a discontinuity. In later work, however, Garnero et al. (1993) concluded, from the triplicated arrival *Scd* and from *ScS-S* differential travel times, that a discontinuity exists under the same region where no discontinuity was found in their previous study (SGHP, Figure 1). Model SGHP (Garnero et al., 1993) shows a discontinuity of ~2.4% and a D" thickness of 180 km. Model RJK2705 (Valenzuela-Wong, 1996; Valenzuela and Wysession, 1998) for a region located near and to the southeast of the one reported in this study (V96 in Figure 1) has a thickness (186 km) that closely agrees with that of SGHP but shows a greater velocity jump (~3.4%) at the top of D" and a lower velocity at the CMB. Just like in this study, they used the decay constant technique. The differing results between their study and ours should not be surprising given the strong heterogeneity of D" on all scales. Garnero et al. (1993) also show evidence for a discontinuity in the west central Pacific to the east of the Mariana Islands and to the north of Vanuatu and the Solomon Islands (G93, Figure 1). The thickness of the basal layer in this region was poorly constrained but appeared to be around 280 km.

Later work (Russell *et al.*, 2001; Avants *et al.*, 2006; Lay *et al.*, 2006; Ohta *et al.*, 2008; and Hutko *et al.*, 2009) used a stacking technique in order to enhance the detection of the triplicated arrival between *S* and *ScS* (or *P* and *PcP*) in the same general region, SGHP, studied by Garnero *et al.* (1993). These studies used earthquakes in the Tonga-Fiji region recorded predominantly by stations in the western United States. Russell *et al.* (2001) found a D″ layer with a thickness of 230 km and a discontinuity for both *P* and *S* waves with velocity increases of 0.75% and 1.7%, respectively. These velocity jumps are somewhat smaller than in D″ underneath circum-Pacific regions (Avants *et al.*, 2006). Russell *et al.* (2001) also found an ultralow velocity zone (ULVZ). Avants *et al.* (2006) found a discontinuous velocity jump followed by two discontinuous velocity drops which they interpreted as a lens of post-perovskite material above a ULVZ. They noticed high variability on scale lengths on the order of 130 km such that the *S* wave velocity increase at the discontinuity varied between 0.5 and 2.3% and the depth of the discontinuity ranged from 2,490 to 2,735 km. Further work (Lay *et al.*, 2006; Ohta *et al.*, 2008) using expanded data sets confirmed these findings. The overall *S* wave velocity structure where the post-perovskite lens has been observed is slightly slower than PREM. Hutko *et al.* (2009) observed a small (0.5%) *P* wave velocity jump at a discontinuity 140 km above the CMB and a ULVZ underneath. Unlike the work carried out by Lay's group (Russell *et al.*, 2001; Avants *et al.*, 2006; Lay *et al.*, 2006; Ohta *et al.*, 2008; and Hutko *et al.*, 2009) using forward modeling of data stacks, Kawai and Geller (2010) followed a waveform inversion approach in the same broad region. They observed shear velocity decreases and increases of 1%–1.5% in the zones from 400 to 500 km and from 300 to 400 km above the CMB, respectively. They also reported 0.5%–1% velocity increases and decreases in the zones from 100 to 200 km and from 0 to 100 km above the CMB, respectively. Sun and Helmberger (2008) modeled *Scd* arrivals in a region of the east central Pacific centered around 2°N, 105°W and obtained a velocity distribution with a 3.5% velocity increase at a discontinuity located 220 km above the core-mantle boundary. Wen (2002) studied the central Pacific using the *SH* components of events in Fiji recorded in the western US and by the MOMA array at epicentral distances ranging from 83 to 108°. He found that a negative velocity gradient of 3% relative to PREM at the bottom 300 km of the mantle fits the data. Wen also studied a MOMA profile sampling D″ under the north Pacific and southern Alaska using SH_{diff} at distances from about 101 to 110° and concluded that PREM satisfactorily explains the observations.

Conclusions

The *S* wave radial velocity structure of the D″ region was determined for a spot of the east central Pacific Ocean centered at 19°N, 132°W. This area falls in the transition from the large low-velocity province beneath the Pacific to the circum-Pacific high-velocity provinces. The technique of the decay constant was applied in the frequency domain to the *S* and S_{diff} waves of an earthquake in the Tonga Islands recorded by the MOMA array in the northeastern United States. Reflectivity synthetic seismograms were generated by forward modeling while trying different models. These included PREM, models with a gradual decrease of the velocity with increasing depth, models with a gradual increase, and a suite of models with a discontinuous increase at the top of D″ followed by a gradual decrease in the form of a complementary error function, consistent with a thermal boundary layer. Care was taken to guarantee the reliability of the models by requiring a good fit of the decay constant in the frequency domain, a correlation coefficient for the least squares fit greater than or equal to 0.9, and a good fit of the time domain waveforms. A couple models were found to fit the decay constant data since the calculated γ falls within one standard deviation of the observed γ. PREM, however, is closer to the actual data points than J738, the model with a discontinuity. Comparison of the waveforms in the time domain also shows PREM to be better and it was chosen as the preferred model. Consequently, D″ at this location is 150 km thick and has a slightly negative velocity gradient with increasing depth. No velocity discontinuity is observed at the top of D″. The *S* wave velocity is relatively low and the temperatures at the base of the mantle are high, but not so much as in the LLVP of the Pacific. The velocity structure is consistent with D″ acting as a thermal boundary layer. Iron enrichment of mantle materials through chemical reactions is also a possibility since it would result in lowered velocities. The downwelling of oceanic slabs is correlated with regions of high velocities in the lowermost mantle and also with the locations of some of the best documented discontinuities. Therefore a discontinuity is not expected in the area of the present study because it is not a subduction zone. Likewise, no subduction has taken place here during the last 180 Myr.

Acknowledgments

Bibliography

Aki K., Richards P.G., 2002, *Quantitative Seismology, Second edition,* University Science Books, Sausalito, California, 700 pp.

Ammon C.J., Lay T., 2007, Nuclear test illuminates USArray data quality, *Eos Trans. AGU, 88,* 37-38, doi:10.1029/2007EO040001.

Anderson D.L., Hart R.S., 1978a, Attenuation models of the Earth, *Phys. Earth Planet. Int., 16,* 289-306.

Anderson D.L., Hart R.S., 1978b, Q of the Earth, *J. Geophys. Res., 83,* 5,869-5,882.

Avants M., Lay T., Russell S.A., Garnero E.J., 2006, Shear velocity variation within the D" region beneath the central Pacific, *J. Geophys. Res., 111,* B05305, doi:10.1029/2004JB003270.

Bataille K., Flatté S.M., 1988, Inhomogeneities near the core-mantle boundary inferred from short-period scattered *PKP* waves recorded at the Global Digital Seismograph Network, *J. Geophys. Res., 93,* 15,057-15,064.

Bataille K., Lund F., 1996, Strong scattering of short-period seismic waves by the core-mantle boundary and the *P*-diffracted wave, *Geophys. Res. Lett., 23,* 2,413-2,416.

Bataille K., Wu R.S., Flatté S.M., 1990, Inhomogeneities near the core-mantle boundary evidenced from scattered waves: A review, *Pure Appl. Geophys., 132,* 151-173.

Bhattacharyya J., Masters G., Shearer P., 1995a, Shear wave attenuation in the mantle from long-period body waveforms (abstract), *International Union of Geodesy and Geophysics XXI General Assembly abstracts,* B403.

Bhattacharyya J., Masters G., Shearer P., 1995b, A Q_b model for the mantle (abstract), *Eos Trans. AGU, 76* (46), Fall Meeting Suppl., F385.

Bolt B.A., Niazi M., Somerville M.R., 1970, Diffracted *ScS* and the shear velocity at the core boundary, *Geophys. J. R. astr. Soc., 19,* 299-305.

Chapman C.H., Phinney R.A., 1972, Diffracted seismic signals and their numerical solution, in *Seismology: Body waves and sources, Methods in computational Physics, 12,* edited by B. A: Bolt, 165-230, Academic Press, New York City, N. Y.

Doornbos D.J., 1983, Present seismic evidence for a boundary layer at the base of the mantle, *J. Geophys. Res., 88,* 3,498-3,505.

Doornbos D.J., Mondt J.C., 1979a, Attenuation of *P* and *S* waves diffracted around the core, *Geophys. J. R. astr. Soc., 57,* 353-379.

Doornbos D.J., Mondt J.C., 1979b, *P* and *S* waves diffracted around the core and the velocity structure at the base of the mantle, *Geophys. J. R. astr. Soc., 57,* 381-395.

Doornbos D.J., Spiliopoulos S., Stacey F.D., 1986, Seismological properties of D" and the structure of a thermal boundary layer, *Phys. Earth Planet. Int., 41,* 225-239.

Durek J.J., Ekström G., 1996, A radial model of anelasticity consistent with long-period surface-wave attenuation, *Bull. Seism. Soc. Am., 86,* 144-158.

Dziewonski A.M., Anderson D.L., 1981, Preliminary reference Earth model, *Phys. Earth Planet. Int., 25,* 297-356.

Dziewonski A.M., Ekström G., Salganik M.P., 1996, Centroid-moment tensor solutions for April-June 1995, *Phys. Earth Planet. Int., 96,* 1-13.

Fischer K.M., Wysession M.E., Clarke T.J., Fouch M.J., Al-Eqabi G.I., Shore P.J., Valenzuela R.W., Li A., Zaslow J.M., 1996, The 1995-1996 Missouri to Massachusetts broadband seismometer deployment, *IRIS Newsletter, XV* (2), 6-9.

Garnero E.J., 2000, Heterogeneity of the lowermost mantle, *Annu. Rev. Earth Planet. Sci., 28,* 509-537.

Garnero E.J., Helmberger D.V., 1995. A very slow basal layer underlying large-scale low-velocity anomalies in the lower mantle beneath the Pacific: Evidence from core phases, *Phys. Earth Planet. Int., 91,* 161-176.

Garnero E.J., Helmberger D.V., 1996, Seismic detection of a thin laterally varying boundary layer at the base of the mantle beneath the central-Pacific, *Geophys. Res. Lett., 23,* 977-980.

Garnero E., Helmberger D., Engen G., 1988, Lateral variations near the core-mantle boundary, *Geophys. Res. Lett., 15,* 609-612.

Garnero E.J., Helmberger D.V., Grand S., 1993, Preliminary evidence for a lower mantle shear wave velocity discontinuity beneath the central Pacific, *Phys. Earth Planet. Int., 79,* 335-347.

Garnero E.J., McNamara A.K., 2008, Structure and dynamics of Earth's lower mantle, *Science, 320,* 626-628.

Helmberger D., Lay T., Ni S., Gurnis M., 2005, Deep mantle structure and the postperovskite phase transition, *Proc. Natl. Acad. Sci., 102,* 17,257-17,263.

Hernlund J.W., Thomas C., Tackley P.J., 2005, A doubling of the post-perovskite phase boundary and structure of the Earth's lowermost mantle, *Nature, 434,* 882-886.

Hutko A.R., Lay T., Revenaugh J., 2009, Localized double-array stacking analysis of *PcP:* D" and ULVZ structure beneath the Cocos plate, Mexico, central Pacific, and north Pacific, *Phys. Earth Planet. Int., 173,* 60-74.

Kawai K., Geller R.J., 2010, Waveform inversion for localized seismic structure and an application to D" structure beneath the Pacific, *J. Geophys. Res., 115,* B01305, doi:10.1029/2009JB006503.

Kennett B. L. N., 1980, Seismic waves in a stratified half space - II. Theoretical seismograms, *Geophys. J. R. Astr. Soc., 61,* 1-10.

Knittle E., Jeanloz R., 1989, Simulating the core-mantle boundary: An experimental study of high-pressure reactions between silicates and liquid iron, *Geophys. Res. Lett., 16,* 609-612.

Knittle E., Jeanloz R., 1991, Earth's core-mantle boundary: Results of experiments at high pressures and temperatures, *Science, 251,* 1,438 - 1,443.

Krüger F., Weber M., Scherbaum M., Schlittenhardt J., 1995, Evidence for normal and inhomogeneous lowermost mantle and core-mantle boundary structure under the Arctic and northern Canada, *Geophys. J. Int., 122,* 637-657.

Lay T., 1989, Structure of the core-mantle transition zone: A chemical and thermal boundary layer, *Eos Trans. AGU, 70,* 49, 54-55, 58-59.

Lay T., Garnero E.J., 2007, Reconciling the postperovskite phase with seismological observations of lowermost mantle structure, in *Post-perovskite: The last mantle phase transition, Geophys. Monogr., 174,* edited by K. Hirose, J. Brodholt, T. Lay and D. Yuen, 129-153, American Geophysical Union, Washington, D. C.

Lay T., Garnero E.J., 2011, Deep mantle seismic modeling and imaging, *Annu. Rev. Earth Planet. Sci., 39,* 91-123.

Lay T., Helmberger D.V., 1983, A lower mantle *S*-wave triplication and the shear velocity structure of D", *Geophys. J. R. Astr. Soc., 75,* 799-837.

Lay T., Hernlund J., Garnero E.J., Thorne M.S., 2006, A post-perovskite lens and D" heat flux beneath the central Pacific, *Science, 314,* 1272-1276.

Lay T., Williams Q., Garnero E.J., 1998, The core-mantle boundary layer and deep Earth dynamics, *Nature, 392,* 461-468.

Lithgow-Bertelloni C., Richards M.A., 1998, The dynamics of Cenozoic and Mesozoic plate motions, *Rev. Geophys., 36,* 27-78.

Loper D.E., Lay T., 1995, The core-mantle boundary region, *J. Geophys. Res., 100,* 6,397-6,420.

Mondt J.C., 1977, *SH* waves: Theory and observations for epicentral distances greater than 90 degrees, *Phys. Earth Planet. Int., 15,* 46-59.

Mori J., Helmberger D.V., 1995, Localized boundary layer below the mid-Pacific velocity anomaly identified from a *PcP* precursor, *J. Geophys. Res., 100,* 20,359-20,365.

Mula A.H.G., 1981, Amplitudes of diffracted long-period *P* and *S* waves and the velocities and *Q* structure at the base of the mantle, *J. Geophys. Res., 86,* 4,999-5,011.

Mula A.H., Müller G., 1980, Ray parameters of diffracted long period *P* and *S* waves and the velocities at the base of the mantle, *Pure Appl. Geophys., 118,* 1,272-1,292.

Murakami M., Hirose K., Kawamura K., Sata N., Ohishi Y., 2004, Post-perovskite phase transition in MgSiO$_3$, *Science, 304,* 855-858.

Nataf H.-C., Houard S., 1993, Seismic discontinuity at the top of D": A world-wide feature?, *Geophys. Res. Lett., 20,* 2,371-2,374.

Ohta K., Hirose K., Lay T., Sata N., Ohishi Y., 2008, Phase transitions in pyrolite and MORB at lowermost mantle conditions: Implications

for a MORB-rich pile above the core-mantle boundary, *Earth Planet. Sci. Lett., 267,* 107-117.

Phinney R.A., Alexander S.S., 1966, *P* wave diffraction theory and the structure of the core-mantle boundary, *J. Geophys. Res., 71,* 5959-5975.

Ricard Y., Richards M., Lithgow-Bertelloni C., Le Stunff Y., 1993, A geodynamic model of mantle density heterogeneity, *J. Geophys. Res., 98,* 21,895-21,909.

Richards M.A., Engebretson D.C., 1992, Large-scale mantle convection and the history of subduction, *Nature, 355,* 437-440.

Russell S.A., Reasoner C., Lay T., Revenaugh J., 2001, Coexisting shear- and compressional-wave seismic velocity discontinuities beneath the central Pacific, *Geophys. Res. Lett., 28,* 2,281-2,284.

Sailor R.V., Dziewonski A.M., 1978, Measurements and interpretation of normal mode attenuation, *Geophys. J. R. Astr. Soc., 53,* 559-581.

Schlittenhardt J., Schweitzer J., Müller G., 1985, Evidence against a discontinuity at the top of D", *Geophys. J. R. Astr. Soc., 81,* 295-306.

Sidorin I., Gurnis M., Helmberger D.V., 1999a, Evidence for a ubiquitous seismic discontinuity at the base of the mantle, *Science, 286,* 1,326-1,331.

Sidorin I., Gurnis M., Helmberger D.V., 1999b, Dynamics of a phase change at the base of the mantle consistent with seismological observations, *J. Geophys. Res., 104,* 15,005-15,023.

Stacey F.D., Loper D.E., 1983, The thermal boundary-layer interpretation of D" and its role as a plume source, *Phys. Earth Planet. Int., 33,* 45-55.

Stein S., Mills J.M. Jr., Geller R.J., 1981, Q^{-1} models from data space inversion of fundamental spheroidal mode attenuation measurements, in *Anelasticity in the Earth, Geodynamics Ser., 4,* edited by F. D. Stacey, M. S. Paterson and A. Nicholas, 39-53, American Geophysical Union, Washington, D. C.

Stein S., Wysession M., 2003, *An introduction to Seismology, earthquakes, and Earth structure,* 498 pp., Blackwell Publishing, Malden, Massachusetts.

Sun D., Helmberger D., 2008, Lower mantle tomography and phase change mapping, *J. Geophys. Res., 113,* B10305, doi:10.1029/2007JB005289.

Turcotte D.L., Schubert G., 2002, *Geodynamics, Second edition,* 456 pp., Cambridge University Press, Cambridge, England.

Valenzuela-Wong R., 1996, Lateral and radial velocity structure at the base of the mantle from diffracted shear waves, Ph. D. thesis, 255 pp., Washington University, St. Louis, Missouri.

Valenzuela R.W., Wysession M.E., 1998, Illuminating the base of the mantle with diffracted waves, in *The core-mantle boundary region, Geodynamics Ser., 28,* edited by M. Gurnis, M. E. Wysession, E. Knittle and B. Buffett, 57-71, American Geophysical Union, Washington, D. C.

Valenzuela R.W., Wysession M.E., Neustadt M.O., Butler J.L., 2000, Lateral variations at the base of the mantle from profiles of digital S_{diff} data, *J. Geophys. Res., 105,* 6,201-6,220.

Van Loenen P.M., 1988, *S* velocity at the base of the mantle from diffracted *SH* waves recorded by the NARS array, M. Sc. thesis, Department of Theoretical Geophysics, Utrecht, The Netherlands, 25 pp.

Walpole R.E., Myers R.H., 1993, *Probability and Statistics for engineers and scientists, Fifth edition,* 766 pp., Macmillan Publishing Company, New York.

Wen L., 2002, An *SH* hybrid method and shear velocity structures in the lowermost mantle beneath the central Pacific and South Atlantic oceans, *J. Geophys. Res., 107,* B3, 2055, doi:10.1029/2001JB000499.

Widmer R., Masters G., Gilbert F., 1991, Spherically symmetric attenuation within the Earth from normal mode data, *Geophys. J. Int., 104,* 541-553.

Williams Q., Garnero E.J., 1996, Seismic evidence for partial melt at the base of Earth's mantle, *Science, 273,* 1,528-1,530.

Wookey J., Dobson D.P., 2008, Between a rock and a hot place: The core-mantle boundary, *Phil. Trans. R. Soc. A, 366,* 4,543-4,557.

Wright C., Lyons J.A., 1981, Further evidence for radial velocity anomalies in the lower mantle, *Pure Appl. Geophys., 119,* 137-162.

Wysession M.E., 1996a, How well do we utilize global seismicity?, *Bull. Seism. Soc. Am., 86,* 1,207-1,219.

Wysession M.E., 1996b, Imaging cold rock at the base of the mantle: The sometimes fate of slabs?, in *Subduction: Top to bottom, Geophys. Monogr. 96,* edited by G. E. Bebout, D. W. Scholl, S. H. Kirby and John P. Platt, 369-384, American Geophysical Union, Washington, D. C.

Wysession M.E., Fischer K.M., Clarke T.J., Al-eqabi G.I., Fouch M.J., Shore P.J., Valenzuela R.W., Li A., Zaslow J.M., 1996. Slicing into the Earth, *Eos Trans. AGU, 77,* 477, 480-482.

Wysession M.E., Lay T., Revenaugh J., Williams Q., Garnero E.J., Jeanloz R., Kellogg L.H., 1998, The D" discontinuity and its implications, in *The core-mantle boundary region, Geodynamics Ser., 28,* edited by M. Gurnis, M. E. Wysession, E. Knittle and B. Buffett, 273-297, American Geophysical Union, Washington, D. C.